Systematic Evaluation of Tumoral ^{99m}Tc-MAA Uptake Using SPECT and SPECT/CT in 502 Patients Before ^{90}Y Radioembolization

Harun Ilhan[1], Anna Goritschan[1], Phillip Paprottka[2], Tobias F. Jakobs[3], Wolfgang P. Fendler[1], Peter Bartenstein[1], Marcus Hacker[1,4], and Alexander R. Haug[1,4]

[1]Department of Nuclear Medicine, University of Munich, Munich, Germany; [2]Institute of Clinical Radiology, University of Munich, Munich, Germany; [3]Department of Diagnostic and Interventional Radiology, Krankenhaus Barmherzige Brüder, Munich, Germany; and [4]Division of Nuclear Medicine, Department of Biomedical Imaging and Image-Guided Therapy, University of Vienna, Vienna, Austria

The aim of this study was to evaluate the ^{99m}Tc-macroaggregated albumin (^{99m}Tc-MAA) uptake of primary and secondary liver tumors in a large patient cohort before ^{90}Y radioembolization. **Methods:** We included 502 patients during the years 2005–2013 (55% male; mean age, 62 ± 11 y), who were examined with ^{99m}Tc-MAA SPECT or SPECT/CT before planned radioembolization. The patients had colorectal cancer (CRC; n = 195, 38.8%), neuroendocrine tumors (NET; n = 77, 15.3%), mammary cancer (MAM; n = 68, 13.5%), hepatocellular carcinoma (HCC; n = 59, 11.8%), cholangiocellular carcinoma (CCC; n = 40, 8.0%), or urologic tumors (URO; n = 14, 2.8%). SPECT with coregistered contrast-enhanced CT or MR imaging and SPECT/CT images of these patients were analyzed using dedicated software with regard to the ^{99m}Tc-MAA uptake of the liver tumors. Regions of interest were drawn around the lesions manually and quantified the uptake of up to 3 lesions per patient and also adjacent healthy liver tissue without evidence of tumor. We quantified maximum and mean counts per pixel and calculated tumor-to-background ratio (TBR). Data are reported as mean ± SD. Lesion uptake was classified as being homogeneously high (grade 1), heterogeneously high (grade 2), equal to that of the liver (grade 3), or low (grade 4). **Results:** Grade 1 uptake was seen in 230 of 1,008 lesions (with the highest rates in sarcoma [47%], MAM [37%], and NET [32%]), grade 2 in 706 lesions (with the highest rates in CRC [77%], HCC [75%], and CCC [74%]), grade 4 in 57 lesions (with the highest rates in pancreatic cancer [17%], sarcoma [SAR] [13%], and MAM [8%]), and grade 3 in only 15 lesions. In quantitative analysis, the mean TBR_{max} of all lesions was 4.8 ± 4.1 (range, 0.2–50.1), with the highest values in HCC (6.0 ± 4.7; range, 1.4–21.6), NET (5.4 ± 4.9; range, 0.8–43.0), pancreatic cancer (4.0 ± 2.8; range, 0.9–12.2), and CCC (4.7 ± 2.9; range, 0.9–11.6), and the lowest values in SAR (3.5 ± 1.8; range, 0.8–2.7) and MAM (3.6 ± 2.2; range, 0.9–11.6). The mean TBR_{mean} was 1.9 ± 1.0 (range, 0.1–7.2), with the highest values in NET (2.2 ± 1.2; range, 0.2–7.2), HCC (2.1 ± 1.2; range, 0.3–6.3), and CCC (2.0 ± 1.0; range, 0.2–6.3) and the lowest values in MAM (1.7 ± 0.8; range, 0.2–4.1), CRC (1.8 ± 0.9; range, 0.4–6.6), and SAR (1.7 ± 1.1; range, 0.3–3.9). **Conclusion:** The ^{99m}Tc-MAA uptake of different tumor entities shows a wide variation, with generally highest values for NET, HCC, and CCC and lowest values for MAM, CRC, and SAR. However, the variation of uptake within the different tumor entities is high.

Key Words: SPECT/CT; radioembolization; MAA uptake; oncology

J Nucl Med 2015; 56:333–338
DOI: 10.2967/jnumed.114.150565

Radioembolization of primary and secondary liver tumors has emerged as a valuable therapy option. In all such patients, scintigraphy is performed after injection of macroaggregated albumin (MAA) labeled with ^{99m}Tc into the hepatic artery, mainly so as to exclude any relevant arteriovenous shunting from the hepatic arteries to the lungs, which may cause radiation-induced pneumonitis after radioembolization. To visualize any shunting to extrahepatic organs such as duodenum or stomach, often an additional SPECT study with or without simultaneous CT is performed (*1,2*). These additional SPECT or SPECT/CT images provide important information about vascularized liver parenchyma and the ^{99m}Tc-MAA uptake of the liver tumors (*3–5*). From a mechanistic point of view, one might expect a higher response to radioembolization of tumors with a high ^{99m}Tc-MAA uptake, as these tumors are likely to receive a higher dose of radiation; conversely, liver tumors with a low ^{99m}Tc-MAA uptake may have a poor response to radioembolization. Consequently, in some cases the recording of ^{99m}Tc-MAA uptake is considered for the dose calculation (*6,7*). However, the precise link between ^{99m}Tc-MAA uptake of liver tumors and the response to radioembolization remains a matter of controversy. In a recent study, no correlation between ^{99m}Tc-MAA uptake of colorectal cancer (CRC) liver metastases and response according to Response Evaluation Criteria in Solid Tumors was found (*8*). In contrast, another study reported a positive correlation between ^{99m}Tc-MAA uptake, radiographic response, and survival in CRC metastases (*5*). In cholangiocellular carcinoma (CCC), survival after radioembolization did not correlate with the degree of ^{99m}Tc-MAA uptake (*9*). On the other hand, ^{99m}Tc-MAA uptake of hepatocellular carcinoma (HCC) has been shown to be predictive of response, progression-free survival, and overall survival after radioembolization with glass microspheres (*10,11*). Responding HCC had almost double the ^{99m}Tc-MAA uptake of nonresponding HCC in that study. Knowledge of the

Received Oct. 27, 2014; revision accepted Dec. 22, 2014.
For correspondence or reprints contact: Alexander R. Haug, Division of Nuclear Medicine, Department of Biomedical Imaging and Image-Guided Therapy, University of Vienna, Währinger Gürtel 18-20, 1090 Vienna, Austria.
E-mail: alexander.haug@meduniwien.ac.at
Published online Feb. 5, 2015.

distribution of ^{99m}Tc-MAA uptake of different primary and secondary liver tumors and its variation within the tumor types seems crucial to elucidate its impact on treatment outcome. However, no systematic analysis of the ^{99m}Tc-MAA uptake of different tumor types or of the variation of ^{99m}Tc-MAA uptake within a single tumor entity has yet been published. Therefore, we compiled our finding of ^{99m}Tc-MAA uptake in a series of 502 patients treated for a wide range of tumor entities.

MATERIALS AND METHODS

Patients

In total, 502 patients (277 male, 225 female; mean age, 62 ± 11 y; range, 29–91 y) were retrospectively included in this study. The local ethics committee waived the approval requirements because of the retrospective nature of this study. All patients were treated with radioembolization between 2005 and 2013 and had been examined previously with contrast-enhanced CT or MR imaging. All patients gave written informed consent to treatment. Patients had CRC (n = 195, 39%), metastases from neuroendocrine tumors (NET; n = 77, 15%), mammary cancer (MAM) (n = 68, 14%), HCC (n = 59, 12%), CCC (n = 40, 8%), urologic tumors (URO; n = 14, 2.8%), pancreatic cancer (PAN; n = 13, 2.6%), malignant melanoma (MM; n = 13, 2.6%), gastrointestinal, non-CRC tumors (GI; n = 10, 2.0%), sarcomas (SAR; n = 6, 1.2%), pulmonary cancer (PUL; n = 4, 0.8%), or tumors of the ear, nose, or throat (ENT; n = 3, 0.6%).

Angiography and Imaging Techniques

All patients were assessed with digital subtraction angiography for analysis and anatomic mapping of the hepatic arteries. All patients underwent scintigraphy of the abdomen and thorax to quantify the liver–lung shunting fraction and additional SPECT or SPECT/CT of the liver within 1 h after injection of 100 MBq of ^{99m}Tc-MAA into the hepatic artery. The right and left hepatic arteries were injected separately whenever feasible to simulate radioembolization; the amount of ^{99m}Tc-MAA was calculated according to the size of the arteries; that is, we applied in a typical patient 65 MBq into the right and 35 MBq ^{99m}Tc-MAA into the left hepatic artery. If the liver had a deviant arterial blood supply, we divided the ^{99m}Tc-MAA to the supplied liver parenchyma. To avoid any unspecific uptake of ^{99m}Tc into the stomach, 600 mg of perchlorate were administered orally before angiography (*12*).

Patients were examined with a dual-head SPECT γ camera (e.cam; Siemens Healthcare) or a dual-head SPECT/CT camera (Symbia T; Siemens Healthcare) with low-energy high-resolution collimators (matrix, 128 × 128, 6° angle steps, 25 s per frame). SPECT data were reconstructed using an iterative method (ordered-subset expectation maximization, 3 iterations, 16 subsets, 1.10-cm full width at half maximum). To delineate the liver tumors, the SPECT images were coregistered with a contrast-enhanced CT or MR scan using dedicated software (Hermes Hybrid Viewer; Hermes Medical Solutions).

Diagnostic CT scans of the neck, thorax, abdomen, and pelvis (100–190 mAs, depending on the scanned organ region; 120 kV; collimation, 2.5 mm; pitch, 1.5) were acquired after intravenous injection of iodine-containing contrast agent (Ultravist 300; Schering, 2.5 mL/s). Initiation of the CT scan was delayed 50 s after contrast injection to depict the portal venous phase of the liver.

MR was performed using a 1.50-T system (Magnetom Avanto, Magnetom Aera; Siemens Healthcare). All patients were investigated in supine position. A phased array coil was used for signal reception. The routine MR protocol consisted of unenhanced T1-weighted gradient-echo (2-dimensional fast low-angle shot) sequences in and out of phase; a single-shot T2-weighted sequence (half-Fourier acquisition single-shot turbo spin-echo); a T1-weighted 3-dimensional gradient-echo sequence with fat suppression (volumetric interpolated breath-hold examination) before and 20, 50, and 120 s (depending on circulation time) after intravenous contrast injection (gadolinium ethoxybenzyl diethylenetriamine pentaacetic acid [Primovist, Eovist]; Bayer Schering Pharma; 25 μmol/kg of body weight); a multishot T2-weighted turbo spin-echo sequence with fat saturation; diffusion-weighted sequences with b-values of 50 and 800 s/mm^2; and, after a delay of 15 min, an additional T1-weighted gradient-echo sequence with fat saturation (2-dimensional fast low-angle shot) and a fat-suppressed T1-weighted volumetric interpolated breath-hold 3-dimensional gradient-echo sequence identical to those performed earlier. Parallel imaging with an acceleration factor of 2 was used for all sequences.

Regions of interest were drawn manually around up to 3 liver lesions, and the maximum and mean counts per pixel were noted. A second region of interest was drawn near the respective liver lesion, and the maximum and mean counts per pixel of healthy liver tissue were noted. This region of interest was drawn close to the lesion to exclude variations due to inhomogeneous ^{99m}Tc-MAA distribution within the liver. The tumor-to-background ratio (TBR) was calculated by dividing the counts per pixel of the tumor by the counts per pixel of the liver. The maximum values were used for the TBR_{max} and the mean values for the TBR_{mean}. Furthermore, we categorized the uptake of the liver tumors as grade 1 (uptake homogenously higher than liver), grade 2 (uptake higher than liver, but inhomogeneous), grade 3 (same uptake as liver), or grade 4 (uptake lower than liver) (Fig. 1).

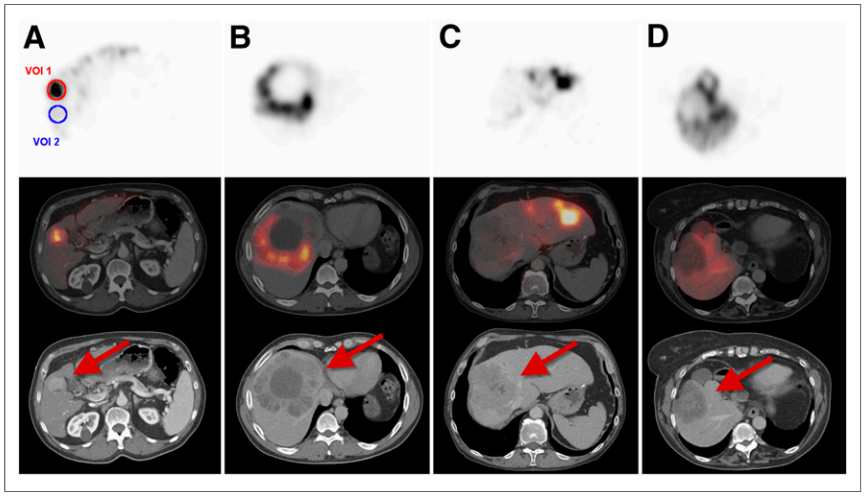

FIGURE 1. Examples of ^{99m}Tc-MAA uptake grades 1 (A), 2 (B), 3 (C), and 4 (D). SPECT images are shown in upper row, CT images in lower row, fused SPECT/CT in middle row. VOI = volume of interest.

Statistical Analysis

Quantitative data were given as mean ± SD and range. Statistical analyses were performed using the SPSS software package (version 21.0; SPSS Inc.). The Kolmogorov–Smirnov test was used to prove gaussian distribution of data. To identify significant differences between TBR values of different tumor entities, we used the Mann–Whitney U test with Bonferroni adjustment for multiple

TABLE 1
Distribution of Uptake Categories in Different Tumor Types

Tumor	Grade 1		Grade 2		Grade 3		Grade 4	
	n	%	*n*	%	*n*	%	*n*	%
HCC	13	16.9	58	75.3	2	2.6	4	5.2
CCC	14	21.5	48	73.8	0	0	3	4.6
MAM	45	36.6	66	53.7	2	1.6	10	8.1
CRC	76	17.2	338	76.5	7	16	21	4.8
NET	57	31.7	108	60.0	4	2.2	11	6.1
PAN	6	25.0	14	58.3	0	0	4	16.7
PUL	3	30.0	7	70.0	0	0	0	0
MM	2	11.1	15	83.3	0	0	1	5.6
URO	5	16.7	25	83.3	0	0	0	0
ENT	0	0	8	100.0	0	0	0	0
GI	2	12.5	13	81.3	0	0	1	6.3
SAR	7	46.7	6	40.0	0	0	2	13.3

Grade 1 = homogeneous high uptake; grade 2 = heterogeneous high uptake; grade 3 = uptake equal to liver uptake; grade 4 = low uptake.

testing. To test for significant differences within the 4 groups of uptake, we used the Kruskal–Wallis test. To test for equal distribution of the uptake categories of the different tumor types, we used the χ-Quadrat test. A statistically significant difference was defined as a P value of less than 0.05.

RESULTS

In total, 1,008 liver lesions were evaluated. Of these, 230 (22.8%) showed grade 1 uptake, 706 (70.0%) grade 2 uptake, 15 (1.5%) grade 3 uptake, and 57 (5.7%) grade 4 uptake. The distribution of the respective uptake categories was significantly different among the tumor types ($P < 0.001$). In all tumor types except SAR, most of the lesions showed grade 2 uptake (Table 1; Fig. 2), with the highest rates in ENT (100%), MM and URO (83.3%), GI (81.3%), CRC (76.5%), HCC (75.3%), and CCC (73.8%). SAR (46.7%), MAM (36.6%), NET (31.7%), and PUL (30%) had the highest rates of grade 1 uptake. PAN (16.7) and SAR (13.3%) had the highest rates of grade 4 uptake. Both TBR_{max} and TBR_{mean} were significantly different among the 4 grades of uptake in the total patient population ($P < 0.001$). Within most tumor types, TBR values differed for the various uptake categories, too. Table 2 provides detailed analysis of the TBR values.

In quantitative analysis of all lesions, the mean $TBR_{mean} \pm SD$ was 1.91 ± 1.01 with a median of 1.68, and the mean TBR_{max} was 4.76 ± 4.09 with a median of 3.59. ENT (2.61), GI (2.27), NET (2.16), HCC (2.13), and CCC (2.05) had the highest TBR_{mean} values, whereas MAM (1.65), SAR (1.73), and CRC (1.80) had the lowest mean values. Regarding TBR_{max}, ENT (6.60), HCC (6.02), MM (5.68), URO (5.41), NET (5.38), PUL (5.10), and CCC (4.70) had the highest values, whereas SAR (3.50) and MAM (3.58) had the lowest values (Table 3).

Interestingly, in the grade 1 uptake group, GI had the highest mean TBR_{mean}, followed by HCC, CCC, SAR, and NET. In the grade 2 uptake group, ENT had the highest TBR_{mean}, followed by PAN, NET, and PUL. In grade 4, the lowest uptake group, MM had the lowest TBR_{mean}, followed by GI and CCC. Regarding the TBR_{max} of the grade 1 group, GI had the highest value, followed by HCC, MM, CCC, and NET. HCC had the highest TBR_{max} in group 2, followed by NET, PUL, MM, and URO.

DISCUSSION

In this comprehensive analysis of the ^{99m}Tc-MAA uptake of different tumor types, we examined more than 1,000 lesions in 502 patients. As expected, HCC, NET, and CCC had quite high uptake values. Interestingly, some other tumors such as ENT, GI, URO, and PAN had TBR values as high as the aforementioned, but the total numbers of lesions in these tumors was much lower; the significance and prognostic value of the relatively high uptake values in these rather rare primary tumors is therefore limited. The SD and range of ^{99m}Tc-MAA uptake was high in all tumor types. Even in tumor types with typically high uptake, there were some tumors with low uptake. On the other hand, even in tumors types with typically low uptake, most had an uptake higher than that of healthy liver parenchyma. The values reported in this study are much lower regarding HCC than those reported by Garin et al. (*10*). This discrepancy might be explained by the mode of ^{99m}Tc-MAA injection: whereas Garin et al. seemed to inject ^{99m}Tc-MAA very selectively in only the tumor-feeding artery, we generally made a less selective injection in our patients. This difference in ^{99m}Tc-MAA application method would naturally have resulted in major differences of uptake in the liver parenchyma and likewise in the tumor, with unpredictable effects on the TBR.

Not surprisingly, MAM and CRC had low uptake values; these tumor entities often appear hypovascularized on contrast-enhanced CT and on angiography (*13*). Supporting our data, almost half the CRC liver metastases in another study had a lower uptake than that of liver parenchyma (*8*). Furthermore, tumor entities presenting with a high TBR, such as HCC and CCC, are

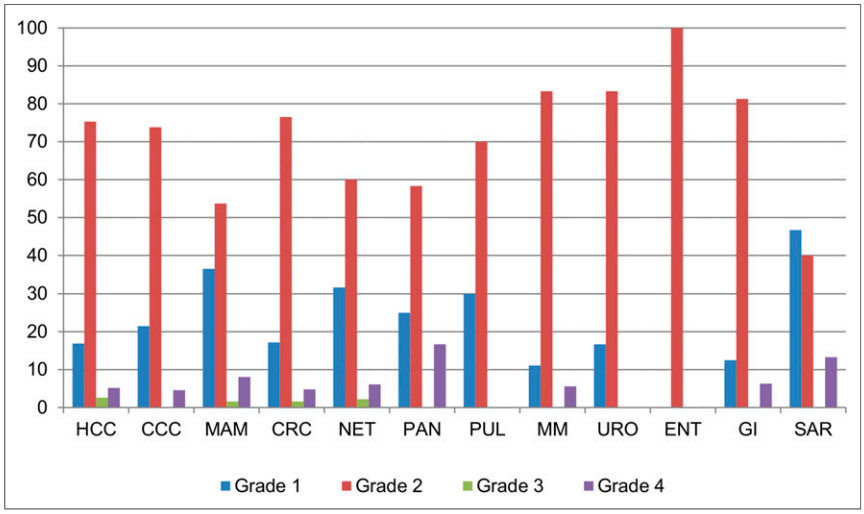

FIGURE 2. Distribution of ^{99m}Tc-MAA uptake categories among different tumor types.

TABLE 2
Analysis of TBR_{max} and TBR_{mean} When Grade 1 and 2 Uptake Was Significantly Different from Grade 3 and 4 Uptake ($P < 0.05$)

		TBR_{mean}			TBR_{max}			
Tumor	Grade	Mean	SD	Median	Mean	SD	Median	*n*
HCC	1	2.56	1.53	2.14	5.70	3.98	4.91	13
	2	2.14	1.17	1.96	6.44	4.92	4.70	58
	3	1.43	0.64	1.43	3.11	2.38	3.11	2
	4	0.62	0.18	0.65	2.54	1.51	2.00	4
CCC	1	2.54	1.53	1.96	4.84	3.86	3.22	14
	2	2.00	0.64	1.93	4.86	2.52	4.04	48
	3							0
	4	0.45	0.22	0.41	1.43	0.78	1.22	3
MAM	1	1.80	0.79	1.55	3.5	2.33	2.85	45
	2	1.70	0.72	1.51	3.78	2.10	3.21	66
	3	0.92	0.15	0.92	3.22	2.85	3.22	2
	4	0.82	0.20	0.91	2.06	2.15	1.42	10
CRC	1	1.99	0.93	1.73	4.14	3.01	3.25	76
	2	1.84	0.90	1.62	4.86	4.17	3.80	338
	3	1.05	0.32	0.98	2.58	1.49	2.14	7
	4	0.73	0.25	0.67	1.98	0.96	1.77	21
NET	1	2.21	0.84	1.89	4.72	2.83	3.84	57
	2	2.32	1.33	1.88	6.15	5.82	4.80	108
	3	1.14	0.29	1.23	3.90	2.37	3.63	4
	4	0.66	0.27	0.69	1.70	0.71	1.63	11
PAN	1	1.60	0.33	1.46	3.03	1.38	2.59	6
	2	2.39	1.26	1.94	5.18	3.04	3.68	14
	3							0
	4	0.76	0.30	0.81	1.61	0.63	1.53	4
PUL	1	1.35	1.06	1.94	2.69	2.17	3.90	3
	2	2.27	0.81	1.97	6.13	4.30	5.13	7
	3							0
	4							0
MM	1	2.15	0.66	2.15	5.11	3.80	5.12	2
	2	2.01	1.14	1.60	6.07	6.28	4.39	15
	3							0
	4	0.22		0.22	0.98		0.98	1
URO	1	1.75	0.59	1.49	3.44	1.44	3.38	5
	2	2.01	0.99	1.79	5.81	7.35	3.47	25
	3							0
	4							0
ENT	1							0
	2	2.61	0.55	2.39	6.60	3.29	5.66	8
	3							0
	4							0
GI	1	4.07	0.04	4.07	8.18	0.87	8.18	2
	2	2.12	0.74	1.92	4.77	2.02	4.68	13
	3							0
	4	0.50		0.50	1.31		1.31	1
SAR	1	2.47	1.15	2.03	4.31	1.90	4.00	7
	2	1.31	0.37	1.40	3.21	1.33	3.62	6
	3							0
	4	0.42	0.11	0.42	1.52	0.56	1.52	2

typically highly vascularized, both on cross-sectional imaging and on angiography. Compared with metastases, these primary liver tumors present with different vascularization features. Especially, HCC tumors often present with a single tumor-feeding artery and thus can be treated in a selective fashion. Therefore, further studies comparing ^{99m}Tc-MAA uptake in primary liver tumors with that in liver metastases are desirable. However, tumor vascularization on cross-sectional imaging and angiography do not necessarily correlate with ^{99m}Tc-MAA uptake. Significant differences between vascularization of tumors as assessed during angiography and ^{99m}Tc-MAA uptake on SPECT are described. Therefore, conclusions derived from contrast enhancement of tumors have to be drawn with caution, especially as results derived from angiography and cross-sectional imaging are contradictory in some cases (*13,14*).

Only a handful of studies have so far tried to link treatment response to ^{99m}Tc-MAA uptake. The fact that tumor uptake has mostly been graded categorically, such as higher than liver or lower than liver, might contribute to the partially discordant results between studies (*8,15*). Even within the categoric groups there are major differences in quantitative ^{99m}Tc-MAA uptake, with a large relative SD, as shown in Table 2. Extensive knowledge of tumoral ^{99m}Tc-MAA uptake within and between the different tumor types seems crucial to the planning of prospective studies with the goal of elucidating the correlation of ^{99m}Tc-MAA uptake, tumor vascularization, and prediction of the effectiveness of radioembolization. Of course, there has been a vociferous debate about the differences in ^{99m}Tc-MAA uptake and uptake after radioembolization as measured by bremsstrahlung SPECT. However, these differences were evaluated in only 31 patients (*16*). Between methods, there are important differences in particle size, as well as the amount and morphology of the embolizing particles. The embolizing effect of treatment with resin microspheres may be a function of arterial blood flow and, consequently, particle distribution or deposition in the tissue. However, the available data are very preliminary, and the number of patients evaluated in this manner remains low.

The present study suffers from some drawbacks. Notably, the data were acquired retrospectively. We commonly found a very heterogeneous ^{99m}Tc-MAA distribution within the liver, a limitation that we tried to overcome by normalizing the tumor uptake by the uptake of adjacent, presumably healthy liver. Especially in primary liver tumors, prior local treatments such as transarterial chemoembolization may have lowered the ^{99m}Tc-MAA uptake, with the typical finding of central necrosis (grade 2 uptake); this may also be true for antiangiogenic treatments in CRC. Since we did not record prior treatments, this limitation may hamper the significance of the present data. Furthermore, especially in patients with disseminated hepatic metastases, undetectable lesions and partial-volume effects may limit the validity of our quantitative TBR analysis. However, combined information derived from SPECT and contrast-enhanced MR imaging and CT increased accuracy.

As a first step toward resolving these issues, we obtained extensive and detailed knowledge of the distribution of ^{99m}Tc-MAA uptake in the treated liver tumors; however, a comparison of ^{99m}Tc-MAA SPECT with bremsstrahlung SPECT or with response and survival data may be highly instructive. As a second step, we hope to obtain data about the link between ^{99m}Tc-MAA uptake, bremsstrahlung SPECT, and survival. As an example, we did perform such a comparison in two patients. The first patient

TABLE 3
Overview of TBR_{mean} and TBR_{max} Values Within Different Tumor Types

		TBR_{mean}				TBR_{max}			
Tumor	*n*	Mean	SD	Range	Median	Mean	SD	Range	Median
HCC	77	2.11	1.24	0.29–6.32	1.88	6.03	4.67	1.43–21.57	4.70
CCC	65	2.05	0.97	0.24–6.26	1.88	4.70	2.87	0.77–14.00	3.85
MAM	123	1.65	0.76	0.17–4.07	1.47	3.58	2.22	0.89–11.56	2.84
CRC	442	1.80	0.92	0.41–6.56	1.59	4.57	3.92	0.95–50.15	3.49
NET	180	2.16	1.21	0.24–7.21	1.85	5.38	4.93	0.85–42.92	3.87
PAN	24	1.93	1.14	0.39–5.45	1.66	4.05	2.79	0.93–12.15	2.99
PUL	10	1.99	0.94	0.12–3.65	1.95	5.10	4.02	0.18–14.18	3.94
MM	18	1.93	1.13	0.22–4.33	1.64	5.68	5.90	0.98–26.54	3.90
URO	30	1.97	0.94	1.04–5.69	1.78	5.41	3.44	1.40–36.72	3.44
ENT	8	2.61	0.55	2.10–3.61	2.39	6.60	3.29	3.44–12.98	5.66
GI	16	2.27	1.05	0.50–4.10	1.96	4.98	2.37	1.31–9.28	4.84
SAR	15	1.73	1.10	0.34–3.90	1.52	3.49	1.77	1.21–6.81	3.45

n = number of lesions.

was a 65-y-old woman with hepatically metastasized MAM (Fig. 3). The 15-mm tumor lesion in the right liver lobe showed a high TBR and grade 1 uptake on ^{99m}Tc-MAA SPECT. Posttherapy bremsstrahlung SPECT, however, showed no increased uptake of resin microspheres. The second patient was a 49-y-old man with liver metastases from nasopharyngeal carcinoma (Fig. 4). The tumor, presenting with central necrosis in the right lobe, showed peripheral high, heterogenic (grade 2) uptake. On bremsstrahlung SPECT after ^{90}Y radioembolization, the tumor still showed a high TBR and grade 2 uptake, although the pattern differed from that of ^{99m}Tc-MAA SPECT, with high uptake in areas that previously had low ^{99m}Tc-MAA uptake and vice versa. More systematic bremsstrahlung analyses have to be performed to obtain more insight into these findings, especially with regard to survival data.

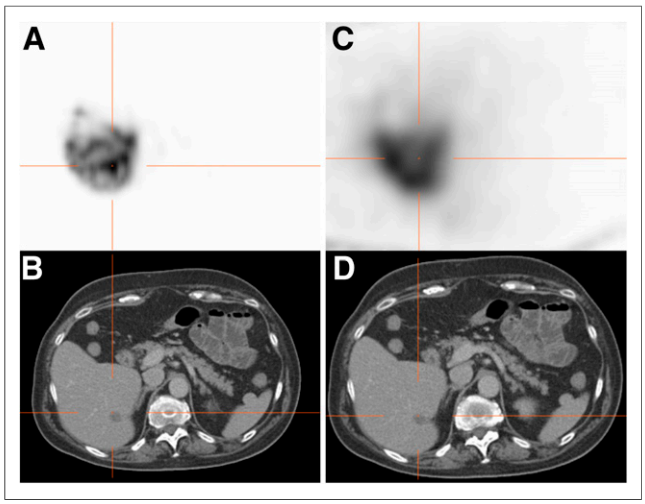

FIGURE 3. ^{99m}Tc-MAA SPECT (A) and SPECT/CT (B) images and post–^{90}Y radioembolization bremsstrahlung SPECT (C) and SPECT/CT (D) images in 65-y-old woman with MAM. Lesions with grade 1 uptake on ^{99m}Tc-MAA SPECT show no uptake on ^{90}Y radioembolization image.

CONCLUSION

The ^{99m}Tc-MAA uptake of different tumor entities is significantly different and varies widely, with the highest values being seen for NET, HCC, and CCC and the lowest for MAM, CRC, and SAR. However, the variation within the particular tumor entities is high.

DISCLOSURE

The costs of publication of this article were defrayed in part by the payment of page charges. Therefore, and solely to indicate this fact, this article is hereby marked "advertisement" in accordance with 18 USC section 1734. No potential conflict of interest relevant to this article was reported.

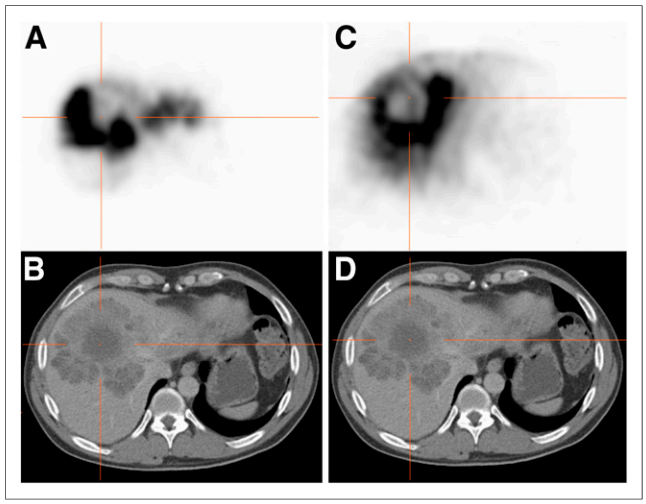

FIGURE 4. ^{99m}Tc-MAA SPECT (A) and SPECT/CT (B) images and post–^{90}Y radioembolization bremsstrahlung SPECT (C) and SPECT/CT images (D) in 49-y-old man with nasopharyngeal carcinoma. Centrally necrotic lesion in right lobe shows grade 2 uptake on ^{99m}Tc-MAA SPECT and bremsstrahlung SPECT; however, distribution and uptake pattern are different.

REFERENCES

1. Hamami ME, Poeppel TD, Muller S, et al. SPECT/CT with ^{99m}Tc-MAA in radioembolization with ^{90}Y microspheres in patients with hepatocellular cancer. *J Nucl Med.* 2009;50:688–692.
2. Ahmadzadehfar H, Sabet A, Biermann K, et al. The significance of ^{99m}Tc-MAA SPECT/CT liver perfusion imaging in treatment planning for ^{90}Y-microsphere selective internal radiation treatment. *J Nucl Med.* 2010;51:1206–1212.
3. Ahmadzadehfar H, Sabet A, Muckle M, et al. ^{99m}Tc-MAA/^{90}Y-bremsstrahlung SPECT/CT after simultaneous Tc-MAA/^{90}Y-microsphere injection for immediate treatment monitoring and further therapy planning for radioembolization. *Eur J Nucl Med Mol Imaging.* 2011;38:1281–1288.
4. Kao YH, Hock Tan AE, Burgmans MC, et al. Image-guided personalized predictive dosimetry by artery-specific SPECT/CT partition modeling for safe and effective ^{90}Y radioembolization. *J Nucl Med.* 2012;53:559–566.
5. Lam MG, Goris ML, Iagaru AH, Mittra ES, Louie JD, Sze DY. Prognostic utility of ^{90}Y radioembolization dosimetry based on fusion ^{99m}Tc-macroaggregated albumin-^{99m}Tc-sulfur colloid SPECT. *J Nucl Med.* 2013;54:2055–2061.
6. Ho S, Lau WY, Leung TW, Chan M, Johnson PJ, Li AK. Clinical evaluation of the partition model for estimating radiation doses from yttrium-90 microspheres in the treatment of hepatic cancer. *Eur J Nucl Med.* 1997;24:293–298.
7. Uliel L, Royal HD, Darcy MD, Zuckerman DA, Sharma A, Saad NE. From the angio suite to the gamma-camera: vascular mapping and ^{99m}Tc-MAA hepatic perfusion imaging before liver radioembolization—a comprehensive pictorial review. *J Nucl Med.* 2012;53:1736–1747.
8. Ulrich G, Dudeck O, Furth C, et al. Predictive value of intratumoral ^{99m}Tc-macroaggregated albumin uptake in patients with colorectal liver metastases scheduled for radioembolization with ^{90}Y-microspheres. *J Nucl Med.* 2013;54: 516–522.
9. Haug AR, Heinemann V, Bruns CJ, et al. ^{18}F-FDG PET independently predicts survival in patients with cholangiocellular carcinoma treated with ^{90}Y microspheres. *Eur J Nucl Med Mol Imaging.* 2011;38:1037–1045.
10. Garin E, Lenoir L, Rolland Y, et al. Dosimetry based on ^{99m}Tc-macroaggregated albumin SPECT/CT accurately predicts tumor response and survival in hepatocellular carcinoma patients treated with ^{90}Y-loaded glass microspheres: preliminary results. *J Nucl Med.* 2012;53:255–263.
11. Kokabi N, Galt JR, Xing M, et al. A simple method for estimating dose delivered to hepatocellular carcinoma after yttrium-90 glass-based radioembolization therapy: preliminary results of a proof of concept study. *J Vasc Interv Radiol.* 2014;25:277–287.
12. Sabet A, Ahmadzadehfar H, Muckle M, et al. Significance of oral administration of sodium perchlorate in planning liver-directed radioembolization. *J Nucl Med.* 2011;52:1063–1067.
13. Sato KT, Omary RA, Takehana C, et al. The role of tumor vascularity in predicting survival after yttrium-90 radioembolization for liver metastases. *J Vasc Interv Radiol.* 2009;20:1564–1569.
14. Kao YH, Tan EH, Teo TK, Ng CE, Goh SW. Imaging discordance between hepatic angiography versus Tc-99m-MAA SPECT/CT: a case series, technical discussion and clinical implications. *Ann Nucl Med.* 2011;25:669–676.
15. Dhabuwala A, Lamerton P, Stubbs RS. Relationship of ^{99m}technetium labelled macroaggregated albumin (^{99m}Tc-MAA) uptake by colorectal liver metastases to response following selective internal radiation therapy (SIRT). *BMC Nucl Med.* 2005;5:7.
16. Wondergem M, Smits ML, Elschot M, et al. ^{99m}Tc-macroaggregated albumin poorly predicts the intrahepatic distribution of ^{90}Y resin microspheres in hepatic radioembolization. *J Nucl Med.* 2013;54:1294–1301.